ACS OMEGA

Open Access

http://pubs.acs.org/journal/acsodf

Article

Enhancing the Cation-Binding Ability of Fluorescent Calixarene Derivatives: Structural, Thermodynamic, and Computational Studies

Katarina Leko,[†] Andrea Usenik,[†] Nikola Cindro, Matija Modrušan, Josip Požar, Gordan Horvat, Vladimir Stilinović, Tomica Hrenar, and Vladislav Tomišić*

Cite This: *ACS Omega* 2023, 8, 43074−43087

Read Online

ACCESS | Metrics & More | Article Recommendations | Supporting Information

ABSTRACT: Novel fluorescent calix[4]arene derivatives **L1** and **L2** were synthesized by introducing phenanthridine moieties at the lower calixarene rim, whereby phenanthridine groups served as fluorescent probes and for cation coordination. To enhance the cation-binding ability of the ligands, besides phenanthridines, tertiary-amide or ester functionalities were also introduced in the cation-binding site. Complexation of the prepared compounds with alkali metal cations in acetonitrile (MeCN), methanol (MeOH), ethanol (EtOH), *N*,*N*-dimethylformamide (DMF), and dimethyl sulfoxide (DMSO) was investigated at 25 °C experimentally (UV spectrophotometry, fluorimetry, microcalorimetry, and in the solid state by X-ray crystallography) and by means of computational techniques (classical molecular dynamics and DFT calculations). The thermodynamic parameters (equilibrium constants and derived standard reaction Gibbs energies, reaction enthalpies, and entropies) of the corresponding reactions were determined. The tertiary-amide-based compound **L1** was found to have a much higher affinity toward cations compared to ester derivative **L2**, whereby the stabilities of the $ML1^+$ and $ML2^+$ complexes were quite solvent-dependent. The stability decreased in the solvent order: MeCN ≫ EtOH > MeOH > DMF > DMSO, which could be explained by taking into account the differences in the solvation of the ligands as well as free and complexed alkali metal cations in the solvents used. The obtained thermodynamic quantities were thoroughly discussed regarding the structural characteristics of the studied compounds, as well as the solvation abilities of the solvents examined. Molecular and crystal structures of acetonitrile and water solvates of **L1** and its sodium complex were determined by single-crystal X-ray diffraction. The results of computational studies provided additional insight into the **L1** and **L2** complexation properties and structures of the ligands and their cation complexes.

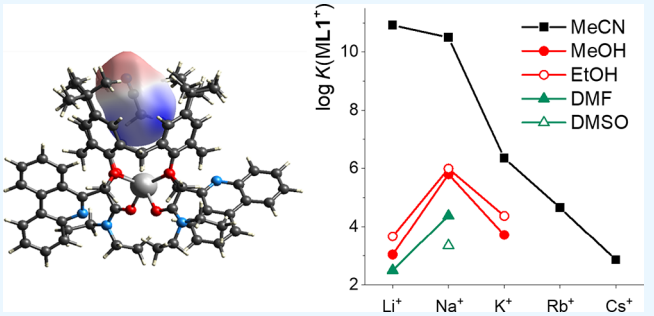

INTRODUCTION

Calixarenes are a class of supramolecular hosts that are readily functionalized at their upper and/or lower rim to give rise to a wide variety of ionophores and molecular receptors and hence have received a great deal of attention in supramolecular chemistry during the past several decades.[1−4] These compounds have found numerous applications not only in chemistry (e.g., catalysis,[5] ion extraction,[6,7] electrochemical[8−10] and fluorescent sensors[11−15]) but also in biological systems (e.g., biomimetics,[16−18] drug-delivery systems,[18,19] and ion channels[20]) and material science.[12,15,21−23]

Among the vast variety of functionalized calixarenes, those functionalized with electron-rich substituents such as carbonyl-containing groups, i.e., amides, esters, and ketones at the lower rim have been extensively studied and were shown to form quite stable complexes with alkali, alkaline-earth, and transition metal cations in various solvents.[6,7,24−34] This is due to a well-defined cation-binding site in which the donor atoms of the calixarene moiety are directed toward the guest. Among the carbonyl group-containing calixarenes, rather basic tertiary amides have been shown to form particularly stable complexes with alkali metal cations, whereas their stabilities are, in general, much lower (though still considerable) in the case of secondary-amide, ester, or ketone derivatives.[24−28,30,35] The affinities of these compounds toward alkali metal cations have been found to be dependent not only on the type of functionalities attached to the carbonyl group but also on the size of the calixarene moiety, i.e., on its compatibility with the cation size.[26,27] Furthermore, the complexation of the cation by calixarene is often greatly influenced by the solvent used, i.e., by the solvation of the cation, macrocycle, and the complex formed.[26−30,33−38] Additionally, the inclusion of solvent molecule in the hydrophobic

Received: August 30, 2023
Revised: October 5, 2023
Accepted: October 11, 2023
Published: November 1, 2023

cavity of both free and complexed ligand can also considerably affect the complexation equilibrium.[28,30,31,33−35,38−40]

Of the many possible approaches for obtaining potentially highly sensitive macrocyclic sensors for a variety of species, one possibility is to introduce fluorescent substituents into the calixarene scaffold. Thus-obtained sensors have received substantial attention in the recent years.[11−14,41−43] The role of fluorescent substituents introduced into the calixarene molecule need not be solely of sensing the binding process, but they can also directly participate in it.[11,12,14,41,42] In the case of cation-binding receptors, this can be achieved if an electron-rich functional group is present in their structure and the fluorescent moiety is adequately positioned for cation coordination. Unlike, e.g., anthracene or naphthalene, the phenanthridine moiety is an example of a group capable of both of these functionalities, since its nitrogen atom can serve as an electron donor and take part in the cation complexation.

We have recently studied the binding of alkali metal cations with calix[4]arene derivatives functionalized with two alternating phenanthridine and methoxy groups as well as four phenanthridine subunits at the lower rim.[41] To enhance the cation-binding ability and solubility in polar organic solvents, in the framework of the present work, we have decided to introduce tertiary-amide and ester functionalities (besides phenanthridine groups) in the cation-binding site. Therefore, the ligands **L1** and **L2** (Figure 1) were synthesized and their

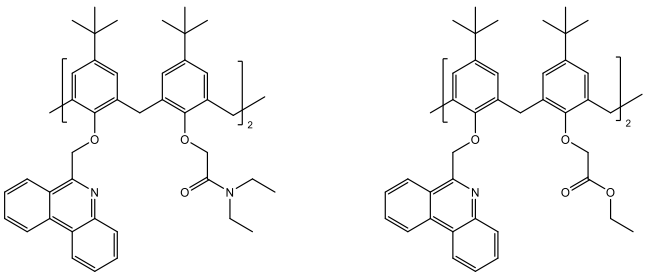

L1 **L2**

Figure 1. Structures of compounds **L1** and **L2**.

complexation with alkali metal cations in acetonitrile (MeCN), methanol (MeOH), ethanol (EtOH), *N,N*-dimethylformamide (DMF), and dimethyl sulfoxide (DMSO) were investigated in detail by means of spectrophotometry, spectrofluorimetry, and microcalorimetry. The effect of solvent on the studied equilibria was particularly addressed. The X-ray solid-state structure determinations of the calixarene **L1** and its sodium complex were carried out as well. Classical molecular dynamics simulations and quantum-chemical calculations related to the properties of macrocycles and their complex species were performed to support the experimental findings and shed light on their possible structures. Such a comprehensive and integrated approach provided quite detailed thermodynamic and structural information about the studied reactions.

EXPERIMENTAL SECTION

Synthesis. All reagents used for the synthesis were purchased from Aldrich, Acros, or Alfa Aesar and were used without further purification. Solvents were distilled before use or dried by the usual methods. NMR spectra were recorded by means of a Bruker Ascend 400 spectrometer with TMS as an internal standard. IR spectra were recorded on a Bruker Vector 22 spectrometer using KBr plates. High-resolution mass spectrometry (HRMS) spectra were recorded on a Bruker Microflex MALDI-TOF spectrometer. Compound **1** (Scheme 1) was prepared by modification of a procedure,[41] which is described in the Supporting Information. 6-(chloromethyl)-phenanthridine hydrochloride was prepared according to the procedure published by Raszeja et al.[44]

***L1** (5,11,17,23-Tetra-tert-butyl-25,27-bis((phenanthridine-6-yl)methoxy)-26,28-di(N,N-diethylaminocarbonyl-methoxy))calix[4]arene).* In 20 cm^3 of anhydrous acetone, compound **1** (1.40 g, 1.38 mmol), potassium carbonate (3.06 g, 22.08 mmol), and 2-bromo-*N,N*-diethylacetamide (2.14 g, 11.04 mmol) were suspended. The reaction mixture was refluxed for 72 h under inert atmosphere. The solvent was evaporated, and the residue was dissolved in 250 mL of dichloromethane and washed 5 times with MiliQ water. The organic layer was passed through a cotton wool and evaporated. Trituration with ethanol resulted in pure product **L1** (1.20 g, 69% yield). The analytical data for compound **L1** are given in the Supporting Information (Figures S1 and S3).

***L2** (5,11,17,23-Tetra-tert-butyl-25,27-bis((phenanthridine-6-yl)methoxy)-26,28-di(ethoxycarbonylmethoxy))calix[4]-arene).* In 25 cm^3 of anhydrous acetone, compound **1** (2.00 g, 1.94 mmol), potassium carbonate (4.30 g, 31.04 mmol), and ethyl bromoacetate (1.72 mL, 2.59 g, 15.52 mmol) were suspended. The reaction mixture was refluxed for 72 h under inert atmosphere. The solvent was evaporated, and the residue was dissolved in 250 mL of dichloromethane and washed 5 times with MiliQ water. The organic layer was passed through cotton wool and evaporated. The precipitate was dissolved in dichloromethane, methanol was added, and the product was filtered to give compound **L2** (670 mg, 29% yield). The analytical data for compound **L2** are given in the Supporting Information (Figures S2 and S4).

Physicochemical Measurements. *Materials.* The salts used to investigate the complexation properties of calixarene derivatives **L1** and **L2** were chosen according to their solubility in particular solvent and were $LiClO_4$ (Sigma-Aldrich, 99.99%), $NaClO_4$ (Sigma-Aldrich 98+ %), $KClO_4$ (Merck, *p.a.*), K[B(Ph)$_4$] (Sigma-Aldrich, 97%), KI (Fluka, 99.0%), RbI (Sigma-Aldrich, 99.9%), and CsI (Merck, 99.5%). 18-crown-6 (Sigma-Aldrich, 99%) and $BaCl_2$ (Sigma-Aldrich, 99.9%) were used for the calorimeter calibration. The solvents, namely, acetonitrile (J. T. Baker, HPLC Gradient grade), methanol (J. T. Baker, HPLC Gradient grade), ethanol (Sigma-Aldrich, Spectranal), *N,N*-dimethylformamide (Honeywell, ≥99.9% for HPLC), and dimethyl sulfoxide (Acros Organics, 99.9% for spectroscopy), were used without further purification for spectrophotometric and microcalorimetric titrations, whereas methanol and ethanol were distilled for fluorimetric experiments, carried out in the lower concentration range, to remove the small amount of interfering cations possibly present in these solvents.

Spectrophotometry. Spectrophotometric titrations were carried out at (25.0 ± 0.1) °C by means of an Agilent Cary 60 spectrophotometer equipped with a thermostatting device. The spectral changes of **L1** and **L2** solutions (V_0 = 2.0 to 2.2 cm^3, c_0 = 1×10^{-4} mol dm^{-3}) were recorded upon stepwise addition of metal salt solution ($c = 1 \times 10^{-3}$ mol dm^{-3} to 1×10^{-1} mol dm^{-3}) directly into the measuring quartz cell (Hellma, Suprasil QX, l = 1 cm). Absorbances were sampled at 1 nm intervals with an integration time of 0.2 s. The titrations for each ligand−cation system were repeated three or four times. The obtained

https://doi.org/10.1021/acsomega.3c06509
ACS Omega 2023, 8, 43074−43087

Scheme 1. Synthesis of Calix[4]arene Derivatives L1 and L2[a]

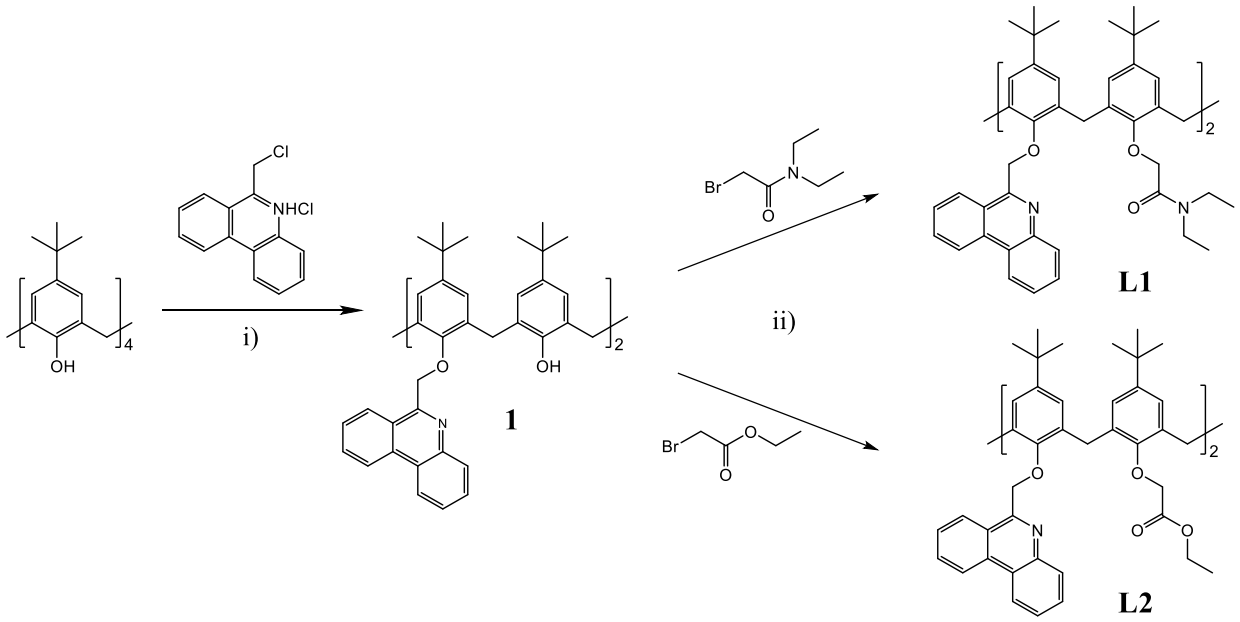

[a]Reagents and conditions: (i) K_2CO_3, NaI, MeCN, Δ, Ar; (ii) K_2CO_3, acetone, Δ, Ar.

spectrophotometric data were processed by HYPERQUAD program package.[45]

Fluorimetry. Fluorimetric experiments were carried out at (25.0 ± 0.1) °C by means of an Agilent Cary Eclipse spectrofluorimeter equipped with a thermostatting device. The spectral changes of **L1** and **L2** solutions (V_0 = 2.5 to 2.6 cm^3, c_0 = 5×10^{-6} to 5×10^{-5} mol dm^{-3}) were recorded upon stepwise addition of metal salt solution ($c = 3 \times 10^{-5}$ mol dm^{-3} to 0.3 mol dm^{-3}) directly into the measuring quartz cell (Agilent, QS, l = 1 cm). Spectra were sampled at 2 nm intervals with an integration time of 0.4 s. The titrations for each ligand/cation system were repeated three or four times. The obtained spectral data were processed by HYPERQUAD program package.[45]

Calorimetry. Microcalorimetric measurements were performed by an isothermal titration calorimeter Malvern Microcal VP-ITC at 25.0 °C. The enthalpy changes obtained upon automated stepwise addition of alkali metal salt solution ($c = 1 \times 10^{-3}$ mol dm^{-3} to 2×10^{-2} mol dm^{-3}) into the ligand solution ($c = 1 \times 10^{-4}$ mol dm^{-3}) were recorded. Blank experiments were performed in order to make corrections for the enthalpy changes of titrant dilution in the pure solvent. The dependence of successive enthalpy change on the titrant volume was processed by nonlinear least-squares fitting procedure using OriginPro 7.0 and OriginPro 7.5 programs, whereas data obtained by competitive titrations were processed by HypDH program.[46] Titrations for each cation/ligand system were repeated at least in triplicate. The calorimeter was calibrated by carrying out the microcalorimetric titrations of 18-crown-6 with $BaCl_2$ at 25.0 °C. The obtained thermodynamic complexation parameters ($\Delta_r H° = (-32.09 \pm 0.05)$ kJ mol^{-1}; $\log K = 3.76 \pm 0.01$) were in excellent agreement with the literature values ($\Delta_r H° = -31.42$ kJ mol^{-1}; $\log K = 3.77$).[47]

X-ray Structure Determination. Single crystals of [Na**L1**]-ClO_4·2MeCN·H_2O were obtained by the slow evaporation of an equimolar acetonitrile solution of $NaClO_4$ and **L1**. The crystal and molecular structures were determined by single-crystal X-ray diffraction. Diffraction measurements were made on an Rigaku Oxford Diffraction XtaLAB Synergy, Dualflex, HyPix X-ray diffractometer with a microfocus sealed PhotonJet (Cu) X-ray source (λ = 1.54184 Å) radiation (**L1**·2MeCN·0.5H_2O) and an Oxford Diffraction Xcalibur Kappa CCD X-ray diffractometer with graphite-monochromated MoK_α (λ = 0.71073 Å) radiation ([Na**L1**]ClO_4·2MeCN·H_2O).[48]

The details concerning the refinement as well as a summary of data pertinent to X-ray crystallographic experiments are provided in the Supporting Information. Further details are available from the Cambridge Crystallographic Centre (CCDC 2006173 and 2076386 contain crystallographic data for this paper).

Computational Methods. The details concerning classical molecular dynamics simulations, conformational analysis, and quantum-chemical calculations are given in the Supporting Information.

RESULTS AND DISCUSSION

Synthesis of Compounds L1 and L2. The synthetic pathway for the preparation of calix[4]arene derivatives **L1** and **L2** is given in Scheme 1. The disubstituted compound **1**,[41] was obtained by addition of 6-(chloromethyl)phenanthridine hydrochloride to *p-tert*-butylcalix[4]arene and was further modified by reaction with 2-bromo-*N*,*N*-diethylacetamide and ethyl bromoacetate to give calix[4]arene derivatives **L1** and **L2**, possessing tertiary-amide or ester groups as parts of the cation-binding sites. Both compounds were prepared in reaction conditions, yielding products solely in the *cone* conformation, which was confirmed by NMR spectroscopy (Figures S1 and S2) and is in agreement with literature data.[2]

The tertiary-amide derivative **L1** was obtained in 69% yield, whereas the reaction yield for the ester-based compound **L2** was 29%. Both calix[4]arene derivatives were characterized by means of NMR spectroscopy, IR, and high-resolution mass spectrometry (Figures S1−S4, Supporting Information).

Crystal Structures and Stereochemistry of L1. Ligand **L1** crystallized as an acetonitrile and water solvate, **L1**·2MeCN·0.5H_2O (Table S1, Figure S5, Supporting Information). The conformation of the calixarene *cone* is of approximate C_4

https://doi.org/10.1021/acsomega.3c06509
ACS Omega 2023, 8, 43074−43087

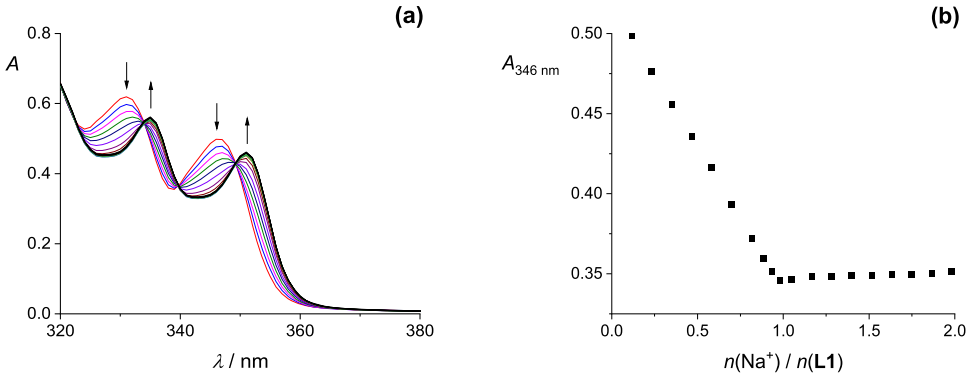

Figure 2. (a) Spectrophotometric titration of **L1** ($c = 1.46 \times 10^{-4}$ mol dm^{-3}) with $NaClO_4$ ($c = 1.50 \times 10^{-3}$ mol dm^{-3}) in MeCN at 25.0 °C; V_0(**L1**) = 2.2 cm^3; l = 1 cm. Spectra are corrected for dilution. (b) Absorbance at 346 nm as a function of cation:ligand molar ratio.

Table 1. Thermodynamic Parameters of Complexation of L1 with Alkali Metal Cations at 25.0 °C

		log K(M**L1**$^+$) ± SE[b]					
solvent	cation[a]	spectrophotometry	fluorimetry	microcalorimetry	$\Delta_r G°$ ± SE (kJ mol^{-1})	$\Delta_r H°$ ± SE (kJ mol^{-1})	$\Delta_r S°$ ± SE (J K^{-1} mol^{-1})
MeCN	Li^+	≳5	≳6	10.92 ± 0.01	−62.32 ± 0.04	−33.66 ± 0.04	96.1 ± 0.3
	Na^+	≳5	≳6	10.50 ± 0.01	−59.88 ± 0.04	−52.09 ± 0.08	26.4 ± 0.4
	K^+	≳5	≳6	6.35 ± 0.02	−36.2 ± 0.1	−32.0 ± 0.2	14 ± 2
	Rb^+	4.63 ± 0.01	4.55 ± 0.02	4.65 ± 0.01	−26.46 ± 0.08	−27.7 ± 0.3	−4 ± 1
	Cs^+	2.85 ± 0.01	2.71 ± 0.02	2.85 ± 0.02	−16.3 ± 0.1	−19.1 ± 0.3	−10 ± 2
MeOH	Li^+	3.15 ± 0.01	3.03 ± 0.02			~0	
	Na^+	≳5	6.12 ± 0.03	5.80 ± 0.03	−33.1 ± 0.2	−30.4 ± 0.2	10 ± 2
	K^+	3.77 ± 0.03	3.54 ± 0.03	3.712 ± 0.003	−21.18 ± 0.02	−23.6 ± 0.2	−7.9 ± 0.6
	Rb^+	3.14 ± 0.01					
EtOH	Li^+	3.75 ± 0.02	3.61 ± 0.01	3.66 ± 0.04	−20.9 ± 0.2	10.5 ± 0.4	104 ± 1
	Na^+	≳5	≳6	5.99 ± 0.02	−34.2 ± 0.1	−22.4 ± 0.3	40 ± 1
	K^+	4.31 ± 0.04	4.37 ± 0.03	4.37 ± 0.01	−24.94 ± 0.05	−16.9 ± 0.4	27 ± 1
DMF	Li^+	2.53 ± 0.02	2.48 ± 0.02	2.49 ± 0.02	−14.22 ± 0.01	−24.9 ± 0.1	−36 ± 3
	Na^+	4.44 ± 0.01	4.48 ± 0.02	4.375 ± 0.004	−25.0 ± 0.2	−43.74 ± 0.03	−63 ± 1
	K^+	1.70 ± 0.01	1.63 ± 0.02				
DMSO	Na^+	3.25 ± 0.03	3.15 ± 0.04	3.340 ± 0.002	−19.07 ± 0.01	−38.8 ± 0.4	−66 ± 1

[a]Complexation of cations other than those listed in the table could not be observed under the conditions used. [b]SE denotes the standard error of the mean (N = 3 or 4).

symmetry (Figure S6a, Supporting Information). The angles of the two phenyl rings with phenanthridine substituents to the mean plane of the macrocycle are quite similar to one another (65.2 and 64.2°), while the two phenyl rings with the amide substituents are at angles of 64.3 and 70.7° to the mean plane of the macrocycle. This conformation of the calixarene *cone* is induced by inclusion of an acetonitrile molecule inside the *cone* with the (electrostatically positive) methyl group of the MeCN inserted into the electron-rich calixarene cavity (Figure S6b,c, Supporting Information).

Molecular Dynamics Studies of L1 and L2 in Solution. Classical molecular dynamics simulations were performed in order to characterize the molecular structures of **L1** and **L2** in the studied solvents.

The results of MD simulations of the ligands in acetonitrile suggested that their affinity for the inclusion of acetonitrile molecules in the calixarene *basket* was high (Figures S7a and S8a, Tables S2 and S3, Supporting Information). **L1**MeCN adduct was present during the entire simulation (Figures S9a and S7a, Table S2, Supporting Information), while the **L2**MeCN adduct was observed during 93% of the simulation time (Figures S10a and S8a, Table S3, Supporting Information).

The formation of methanol adducts of **L1** and **L2** was also observed. During the entire MD simulation of **L1**, its *basket* was occupied (Figures S9b and S7b, Table S2, Supporting Information) by a solvent molecule. Ligand **L2** showed weaker affinity for inclusion of methanol (Figures S10c and S8b, Table S3, Supporting Information).

In DMF **L1** ligand during 45% of the simulation time existed in the form of **L1**DMF adduct in which the methyl group *trans* oriented to the DMF oxygen atom occupied the hydrophobic cavity (Figure S9d, Table S2, Supporting Information), while in a small portion of simulation time (1%) **L1**DMF' adduct was observed, in which the *cis* oriented methyl group was present in the calixarene *cone* (Figure S9e, Table S2, Supporting Information).

The conformation of free calixarene *basket* had a flattened *cone* shape of C_2 symmetry, whereas upon inclusion of acetonitrile or methanol molecule the shape of the *basket* changed to the C_4 symmetrical regular *cone* and slightly flattened *cone* in the case of **L1**DMF adduct. These changes were reflected in the values of the interatomic distances between opposing aryl carbon atoms connected to the *tert*-butyl groups on the calixarene upper rim (Tables S2 and S3, Supporting Information). In the flattened *cone* conformation these values differed significantly, whereas in the regular *cone* conformation they were approximately the same.

https://doi.org/10.1021/acsomega.3c06509
ACS Omega 2023, 8, 43074−43087

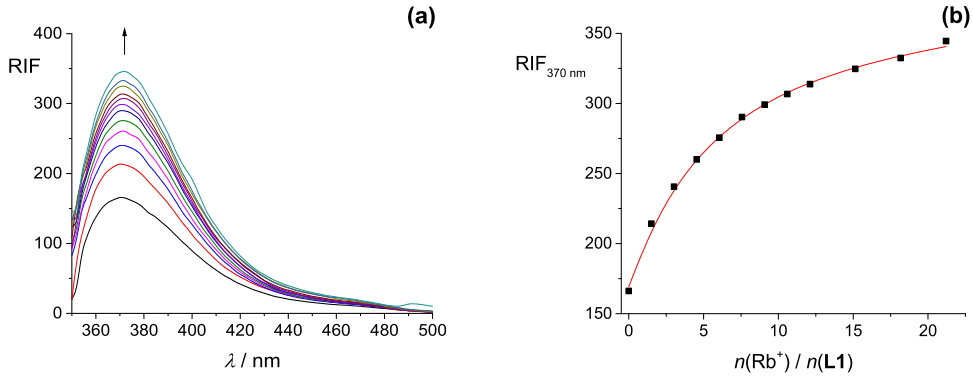

Figure 3. (a) Fluorimetric titration of **L1** ($c = 4.61 \times 10^{-6}$ mol dm^{-3}) with RbI ($c = 3.49 \times 10^{-4}$ mol dm^{-3}) in MeCN at 25.0 °C; V_0(**L1**) = 2.50 cm^3; l = 1 cm.; λ_{ex} = 330 nm; excitation slit 20 nm, emission slit 20 nm. Spectra are corrected for dilution. (b) Relative intensity of fluorescence at 370 nm as a function of cation:ligand molar ratio. ■ experimental; — (red) calculated.

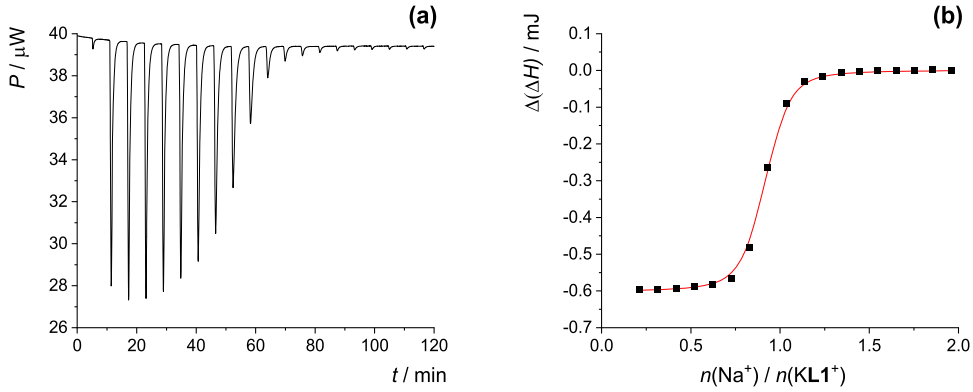

Figure 4. (a) Microcalorimetric competitive titration of K**L1**$^+$ ($c = 2.01 \times 10^{-4}$ mol dm^{-3}, V = 1.42 mL) with $NaClO_4$ ($c = 1.96 \times 10^{-3}$ mol dm^{-3}) in MeCN at 25.0 °C; (b) Dependence of successive enthalpy change on cation:K**L1**$^+$ molar ratio. ■ experimental; — (red) calculated.

In the MD simulations of calixarenes in ethanol and DMSO no formation of solvent adducts was observed (Tables S2 and S3, Supporting Information).

Cation Complexation Thermodynamics: L1. The UV spectral changes recorded upon stepwise addition of $NaClO_4$ in the solution of compound **L1** in acetonitrile are shown in Figure 2, whereas the data obtained in the course of spectrophotometric titrations with other alkali metal salts are given in the Figures S11−S14, Supporting Information. Several neat isosbestic points can be observed in all cases. The spectra correspond to the absorption of phenanthridine moieties, and the observed significant spectral changes could indicate the involvement of phenanthridine subunits in the cation coordination (see later in the article for a further discussion).

Spectrophotometric titration curves of **L1** with $LiClO_4$, $NaClO_4$, and $KClO_4$ in MeCN exhibited a linear change in absorbance depending on the amount of cation added up to the equimolar ratio, followed by a break in the titration curve (Figures 2b, S11b and S12b, Supporting Information). This revealed the formation of 1:1 complexes of high stability constants, which could be assessed to be higher than 10^5 (Table 1). Due to the lower affinity of calixarene derivative **L1** toward larger rubidium and cesium cations, stability constants of Rb**L1**$^+$ and Cs**L1**$^+$ complexes could be determined by processing the spectrophotometric titration data (Table 1, Figures S13 and S14, Supporting Information). Fluorimetric titrations of ligand **L1** with alkali metal cations in acetonitrile were carried out as well and the results are presented in Figures 3 and S15−S18, Supporting Information. The addition of alkali metal salts into the macrocycle solution led to the fluorescence increase as a result of the complexation process. That can be explained by suppression of photoinduced electron transfer (PET), and consequently of fluorescence quenching, upon cation binding, as described in ref 41.

As in the case of previously described spectrophotometric experiments, stability constants of Li**L1**$^+$, Na**L1**$^+$, and K**L1**$^+$ were too high for reliable determination by means of fluorimetry (Figures S15−S17, Supporting Information) and were determined by means of direct and competitive microcalorimetric titrations (Table 1, Figures 4, S20 and S21, Supporting Information) which enabled complete thermodynamic characterization of the cation coordination reactions. The equilibrium constants obtained microcalorimetrically for Rb**L1**$^+$ and Cs**L1**$^+$ formation reactions (Figures S22 and S23, Supporting Information) were in very good agreement with those determined by absorption and emission spectrometry (Table 1).

To confirm the reliability of the thermodynamic data obtained, we also determined complexation enthalpies by direct titrations. As can be seen from the data listed in Table 1 and Table S4 (Supporting Information), the values of reaction enthalpies measured directly and obtained by competitive titrations are in very good agreement.

The highest stability of Li**L1**$^+$ complex in MeCN is a consequence of rather favorable enthalpic ($\Delta_r H° = -33.66$ kJ mol^{-1}) and entropic contributions ($T\Delta_r S° = 28.65$ kJ mol^{-1}) to the standard complexation Gibbs energy. Like in the case of the other calix[4]arene derivatives with carbonyl functional groups at the lower rim,[26,29−31] formation of Na**L1**$^+$ was the most

https://doi.org/10.1021/acsomega.3c06509
ACS Omega 2023, 8, 43074−43087

enthalpically favorable among all studied reactions in this solvent, and that can be rationalized by the compatibility of the sodium cation and macrocycle cation-binding site sizes. Although the stabilities of Na**L1**$^+$ and Li**L1**$^+$ are similar, the standard enthalpies and entropies of the corresponding binding processes differ significantly (Table 1). This can be, at least partially, explained by considering the thermodynamic functions of Na^+ and Li^+ solvation in acetonitrile. Namely, desolvation of Na^+ is less energetically demanding than the same process for Li^+: $\Delta_{sol}H°(Li^+) = -539$ kJ mol^{-1}, $\Delta_{sol}H°(Na^+) = -429$ kJ mol^{-1}, whereas the opposite holds for the desolvation entropies: $\Delta_{sol}S°(Li^+) = -253$ J K^{-1} mol^{-1} , $\Delta_{sol}S°(Na^+) = -206$ J K^{-1} mol^{-1}.[49] The stability constant of K**L1**$^+$ in acetonitrile is more than 4 orders of magnitude lower than that of Li^+ and Na^+ complexes. This is a consequence of the less favorable complexation enthalpy and entropy. The same conclusion holds for the complexation of the Rb^+ and Cs^+ cations.

As mentioned in the Introduction, solvation of both reactants and products participating in complexation can profoundly affect the binding process. In order to investigate the solvent effect on the complexation equilibria, the cation complexation with **L1** was, aside acetonitrile, addressed in methanol, ethanol, *N*,*N*-dimethylformamide and in dimethyl sulfoxide. The solvent choice was made based on the differences in the cation, ligand, and complex solvation abilities, related with the differences in their inter- and intramolecular interactions and properties such as dielectric constants and dipole moments.

The results of spectrophotometric titrations of **L1** with alkali metal cations in methanol are given in the Supporting Information (Figures S24−S27) and Table 1. Due to the poor solubility of cesium salts in MeOH, and the weakest affinity of the ligand **L1** toward this cation, the corresponding stability constant could not be determined by this method. The fluorimetric titrations of **L1** with Li^+, Na^+, and K^+ led to a rather large increase in the ligand fluorescence intensity (Figures S28−S30, Supporting Information), and the equilibrium constants determined by processing the corresponding data are listed in Table 1. A reliable value of the Rb**L1**$^+$ complex stability constant could not be determined fluorimetrically. The results of microcalorimetric investigations of the reactions in methanol are also given in the Supporting Information (Figures S32 and S33) and Table 1. The binding of Li^+ could not be characterized calorimetrically because of the very low heat effects accompanying this process. Similarly, the large enthalpy changes of rubidium salt dilution in methanol prevented the reliable determination of standard thermodynamic parameters by this method.

By comparing the obtained thermodynamic data (Table 1), a huge difference in ligand **L1** affinity toward alkali metal cations in methanol and acetonitrile can be noticed. The strong decrease in stability of lithium complex in methanol can be attributed to the considerably stronger cation solvation with respect to acetonitrile ($\Delta_tH°(Li^+$, MeCN → MeOH) = −13.7 kJ mol^{-1}, $\Delta_tS°(Li^+$, MeCN → MeOH) = 86 J K^{-1} mol^{-1}, $\Delta_tG°(Li^+$, MeCN → MeOH) = −21 kJ mol^{-1}).[49] Namely, because of its considerable charge density, the lithium cation can reorient the solvent dipoles most strongly among the alkali metal cations, even beyond the primary solvation sphere, so a larger number of solvent molecules become released into the bulk upon lithium complexation compared to the reactions of the ligand with other alkali metal cations. Therefore, in the case of Li^+ reaction, its desolvation significantly decreases the absolute value of complexation enthalpy which results in almost isoenthalpic binding process (Table 1). Although the entropy of Li^+ desolvation is rather high, the overall effect of this process is reflected in almost 8 orders of magnitude lower Li**L1**$^+$ stability constant in methanol than in acetonitrile. The complexation of **L1** with Na^+ is an enthalpically and entropically advantageous process in MeOH (as is in MeCN), however the complexation in acetonitrile is much more exothermic ($\Delta(\Delta_rH°) = -21.7$ kJ mol^{-1}). The lower K**L1**$^+$ complex stability in MeOH compared to MeCN, and also with respect to Na**L1**$^+$, is a consequence of both less favorable enthalpic and entropic contributions to the standard reaction Gibbs energy of the complex formation.

Apart from the above considerations, according to the MD results (see below), the energetically favorable inclusion of solvent molecule in the complexed-calixarene *cone* is more pronounced in the case of acetonitrile than for methanol, which additionally increases the difference in the ligand affinity for cations in the two solvents.[35]

The results of experimental studies of complexation of ligand **L1** with alkali metal cations in ethanol are presented in the Supporting Information (Figures S34−S42) and Table 1. Due to the insufficient solubility of rubidium and cesium salts, the investigation of the affinity of ligand **L1** toward these cations could not be carried out. The spectral changes observed in the course of spectrometric measurements regarding binding of Li^+, Na^+, and K^+ were similar to those recorded in acetonitrile and methanol, and again, the addition of cations into ligand solution resulted in the increase of fluorescence intensity. As expected, there are no large differences in complex stabilities in EtOH and MeOH, contrary to MeCN.[30] It is interesting to note that among all of the studied solvents and cations only the reaction of Li^+ with compound **L1** in ethanol is endothermic. This can be again explained by particularly strong solvation of this cation in this solvent. Ligand **L1** binds K^+ more strongly than Li^+, which is by large a consequence of a far more favorable enthalpic contribution to $\Delta_rG°$ in the case of the former cation.

By comparing the values of standard thermodynamic complexation parameters obtained for reaction of Na^+ and K^+ with **L1** in methanol and ethanol, it can be deduced that an interplay between enthalpy and entropy contributions leads to similar standard reaction Gibbs energies for Na**L1**$^+$ formation in these alcohols (enthalpy−entropy compensation). We have reported similar behavior in the case of ketone calix[4]arene derivative.[30] The differences among standard complexation parameters for Na^+ and K^+ complexation in studied alcohols cannot be explained solely on the basis of thermodynamic functions of free cation transfer: $\Delta_tH°$(MeOH → EtOH)/kJ mol^{-1} = 1.3 (Na^+), −0.6 (K^+); $\Delta_tS°$(MeOH → EtOH)/J K^{-1} mol^{-1} = −4.0 (Na^+), −6.0 (K^+).[49] The cation solution enthalpy is almost the same in both solvents, whereas methanol is a better medium for cation solvation in terms of entropy, which in part accounts for the entropically more favorable complexation in ethanol.

The results of spectrophotometric, fluorimetric, and microcalorimetric titrations of ligand **L1** with alkali metal cations in DMF and DMSO are given in the Supporting Information (Figures S43−S53). The Na**L1**$^+$ complex in DMF is significantly more stable than K**L1**$^+$ and Li**L1**$^+$, which is a consequence of the most favorable reaction enthalpy (Table 1). The notable lower **L1** binding affinity for the cations in *N*,*N*-dimethylformamide compared to acetonitrile and examined alcohols is largely due to the more favorable cation solvation in the former solvent relative to the latter: $\Delta_tG°$/kJ mol^{-1}: MeCN → DMF: −35 (Li^+), −25 (Na^+), −18 (K^+); MeOH → DMF: −14 (Li^+), −18 (Na^+), −20

https://doi.org/10.1021/acsomega.3c06509
ACS Omega 2023, 8, 43074−43087

Table 2. Thermodynamic Parameters of Complexation of L2 with Alkali Metal Cations at 25.0 °C[b]

		log $K(\mathbf{ML2}^+) \pm$ SE[b]					
solvent	cation[a]	spectrophotometry	fluorimetry	microcalorimetry	$\Delta_r G° \pm$ SE (kJ mol^{-1})	$\Delta_r H° \pm$ SE (kJ mol^{-1})	$\Delta_r S° \pm$ SE (J K^{-1} mol^{-1})
MeCN	Li^+	≳5	5.6 ± 0.1	5.678 ± 0.002	−32.41 ± 0.01	−26.9 ± 0.1	18.5 ± 0.4
	Na^+	≳5	≳6	5.98 ± 0.01	−34.14 ± 0.07	−45.6 ± 0.4	−39 ± 1
	K^+	3.004 ± 0.006	2.92 ± 0.03	3.069 ± 0.001	−17.52 ± 0.01	−19.7 ± 0.2	−7.4 ± 0.8
MeOH	Na^+	2.71 ± 0.01	2.71 ± 0.01	2.81 ± 0.02	−16.05 ± 0.09	−16.9 ± 0.3	−2.9 ± 0.8
EtOH	Na^+	2.82 ± 0.01	2.89 ± 0.01				

[a]Complexation of cations other than those listed in the table could not be observed under the conditions used. [b]SE denotes the standard error of the mean (N = 3 or 4).

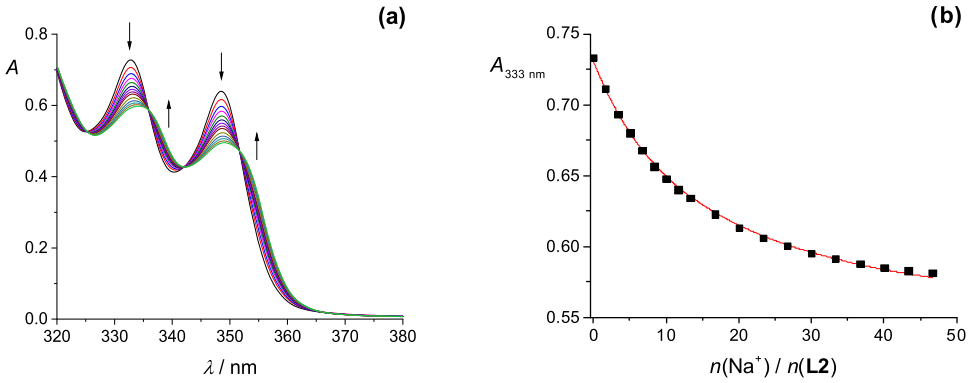

Figure 5. (a) Spectrophotometric titration of **L2** ($c = 1.54 \times 10^{-4}$ mol dm^{-3}) with $NaClO_4$ ($c = 1.81 \times 10^{-2}$ mol dm^{-3}) in MeOH at 25.0 °C; $V_0(\mathbf{L2})$ = 2.2 cm^3; l = 1 cm. Spectra are corrected for dilution. (b) Absorbance at 333 nm as a function of cation-to-ligand molar ratio. ■ Experimental; — calculated.

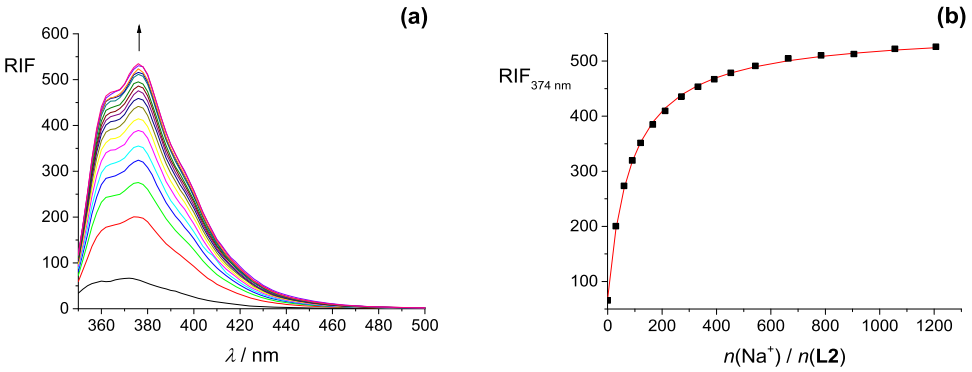

Figure 6. (a) Fluorimetric titration of **L2** ($c = 1.54 \times 10^{-5}$ mol dm^{-3}) with $NaClO_4$ ($c = 0.116$ mol dm^{-3}) in EtOH at 25.0 °C; $V_0(\mathbf{L2})$ = 2.5 cm^3; λ_{ex} = 330 nm; excitation slit 10 nm, emission slit 10 nm. Spectra are corrected for dilution. (b) Relative intensity of fluorescence at 374 nm as a function of cation:ligand molar ratio. ■ experimental; — (red) calculated.

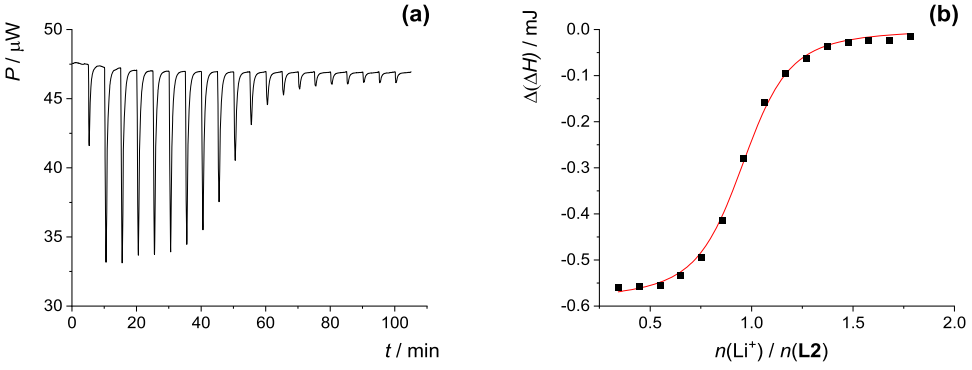

Figure 7. (a) Microcalorimetric titration of **L2** ($c = 1.49 \times 10^{-4}$ mol dm^{-3}, V = 1.42 mL) with $LiClO_4$ ($c = 1.45 \times 10^{-3}$ mol dm^{-3}) in MeCN at 25.0 °C; (b) Dependence of successive enthalpy change on cation:ligand molar ratio. ■ experimental; — (red) calculated.

https://doi.org/10.1021/acsomega.3c06509
ACS Omega 2023, 8, 43074−43087

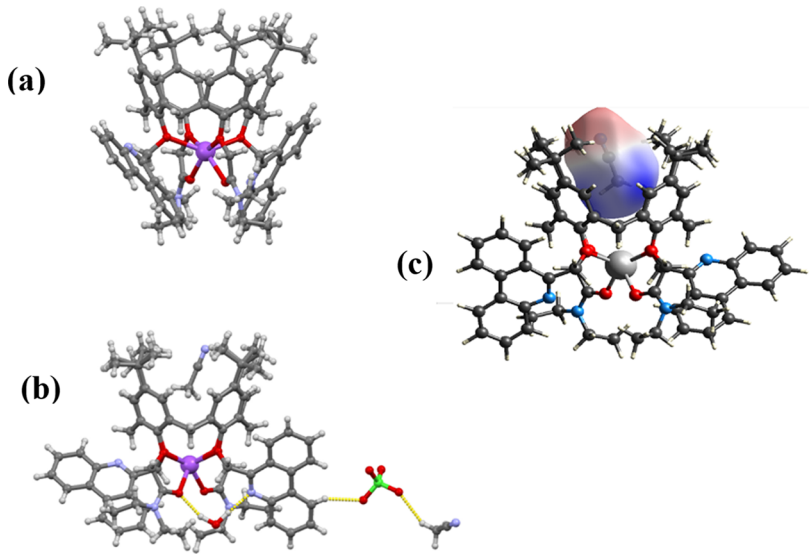

Figure 8. $[NaL1]^+$ complex in the crystal structure of $[NaL1]ClO_4{\cdot}2MeCN{\cdot}H_2O$: (a) with solvent molecules and counterion omitted for clarity; (b) showing the hydrogen bonded water, included acetonitrile molecule and C−H···O bonded perchlorate, as well as the second MeCN molecule; (c) electrostatic potential plotted on the Hirshfeld surface of the MeCN molecule included in the calixarene *cone*.

(K^+); EtOH → DMF: −21 (Li^+), −24 (Na^+), −26 (K^+).[49] Interestingly, the Li^+ and Na^+ complexation entropies in DMF are negative, while the opposite holds for the corresponding reactions in MeCN, MeOH, and EtOH. The trend is consistent with the entropically most beneficial free cation solvation in DMF $\Delta_tS°$/J K^{-1} mol^{-1}: MeCN → DMF: 59.0 (Li^+), 19.8 (Na^+), 17.4 (K^+); MeOH → DMF: 31.3 (Li^+), 19.9 (Na^+), 7.8 (K^+); EtOH → DMF: 49.3 (Li^+), 32.9 (Na^+), 26.8 (K^+).[49]

In dimethyl sulfoxide, solely the binding of Na^+ cation by **L1** was observed (Table 1). This can be again at least partly explained by the favorable alkali metal cation solvation in this solvent, even more than in DMF ($\Delta_tG°$ (Na^+, DMF → DMSO) = −3 kJ mol^{-1}).[49]

Cation Complexation Thermodynamics: L2. Complexation properties of the calix[4]arene derivative **L2** comprising ester and phenanthridine functionalities were investigated in acetonitrile, methanol, and ethanol (Table 2, Figures 5−7 and S54−S67, Supporting Information), whereas no cation binding was observed in *N*,*N*-dimethylformamide and dimethyl sulfoxide under the experimental conditions used. The absorption spectrum of **L2** acetonitrile solution changed very slightly upon addition of Rb^+ and Cs^+ salts (Figures S57 and S58, Supporting Information), indicating low affinity of the ligand for these cations.

The thermodynamic parameters of the reactions of **L2** with Li^+, Na^+, and K^+ in acetonitrile determined by processing the experimental data (Table 2) reveal that the rather high stability of $LiL2^+$ arises from enthalpically and entropically advantageous cation coordination. The highest stability of $NaL2^+$ in MeCN is due to the most favorable $\Delta_rH°$ value among all of the studied complexation processes. The binding of K^+ is less energetically advantageous when compared to sodium but accompanied by less unfavorable entropy change.

By comparing the results of the study of cations complexation by **L2** in methanol (Table 2, Figures 5, S65 and S66, Supporting Information) with those obtained in acetonitrile (Table 2), the considerable reduction in receptor affinity in the former solvent compared to the latter can be noticed, and the same was observed in the case of **L1** and other carbonyl-containing calix[4]arene derivatives.[26,28,30,40] In fact, in MeOH only the formation of the $NaL2^+$ complex could be observed under the experimental conditions used. The huge decrease in **L2** binding ability in methanol can be again rationalized by particularly strong solvation of smaller cations (Li^+ and Na^+) in this solvent as well as the possibility of intermolecular (solvent−ligand) hydrogen bonds formation. As already mentioned in the case of **L1**, the higher affinity of the **L2** complexes for inclusion of MeCN compared to the MeOH molecule (see MD results below) also contributes to the higher cation-binding ability of the ligand in the former solvent relative to the latter.

The results of experimental investigations concerning the cation complexation with **L2** in ethanol are presented in Table 2. As can be seen, solely the binding of sodium cation in this alcohol was observed. The corresponding standard reaction parameters could not be determined calorimetrically, since the enthalpy changes recorded for dilution of sodium salt solutions in EtOH were too high. However, the $NaL2^+$ stability constant was determined by processing the results of the spectrophotometric and fluorimetric titrations. The obtained value is quite close to that determined in MeOH. Therefore, the compound **L2** behaves rather similarly to **L1** and previously investigated ketone calix[4]arene derivative.[30]

Comparison of the stability constants listed in Tables 1 and 2 reveals that the cation-binding ability of **L1** is much larger than that of **L2** in all of the solvents examined. That is in fact expected by taking into account the higher basicity of the tertiary-amide carbonyl oxygen atom with respect to the ester one and is supported by the results of computational studies (see below).

Crystal Structure and Stereochemistry of $[NaL1MeCN]ClO_4$. As in the case of free **L1** (Figure S5), its sodium complex also crystallized as an acetonitrile and water solvate, $[NaL1]ClO_4{\cdot}2MeCN{\cdot}H_2O$ (Figures 8b and S69, Supporting Information). The conformation of the calixarene *cone* is of approximate C_4 symmetry. Similarly, as in the noncoordinated **L1**, the angles of the two phenyl rings with phenanthridine substituents to the mean plane of the macrocycle are almost identical (66.6 and 66.7°), while the two phenyl rings with the amide substituents are at angles of 62.9 and 69.2°

https://doi.org/10.1021/acsomega.3c06509
ACS Omega 2023, 8, 43074−43087

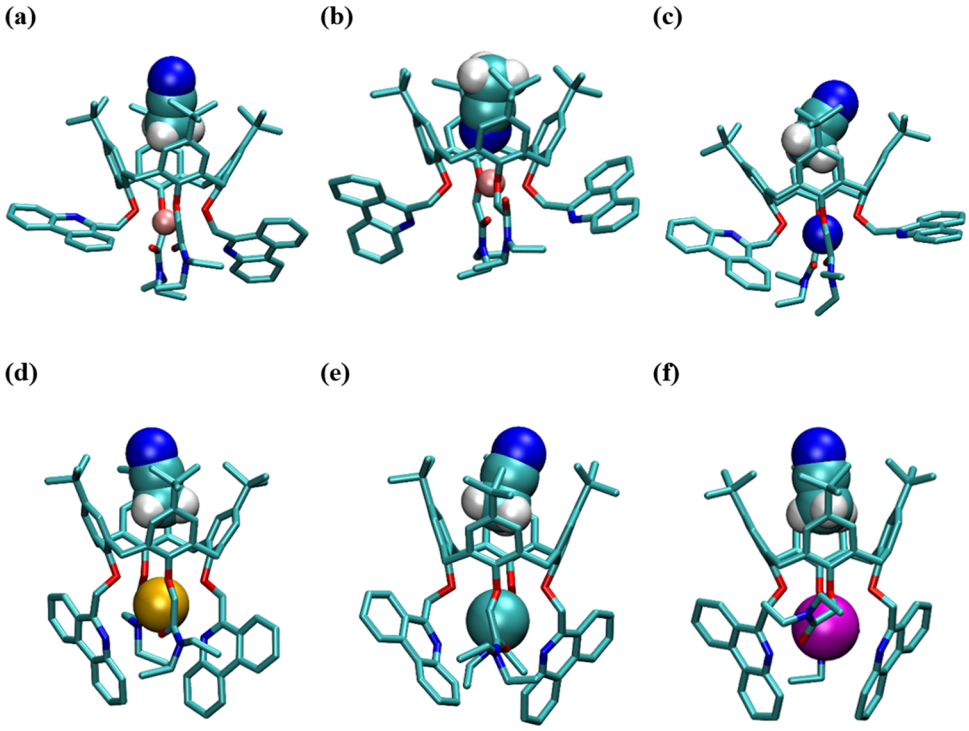

Figure 9. Structures of (a) Li**L1**MeCN$^+$, (b) Li**L1**MeCN′$^+$, (c) Na**L1**MeCN$^+$, (d) K**L1**MeCN$^+$, (e) Rb**L1**MeCN$^+$, and (f) Cs**L1**MeCN$^+$ adducts obtained by MD simulations at 25 °C. Hydrogen atoms of **L1** are omitted for clarity.

to the mean plane of the macrocycle. The sodium atom is hexacoordinated by the four calixarene ether and two ester carbonyl oxygen atoms, forming an extremely distorted trigonal prism (Figure 8). The ether oxygen atoms are almost perfectly coplanar (deviating by only ca 0.01 Å from the mean plane). The sodium atom is placed 0.79 Å below the mean plane of the ether oxygen atoms, with Na−O(ether) bond lengths ranging from 2.3116(18) to 2.5059(18) Å. In calixarenes with amide groups as lower-rim substituents these Na−O(ether) bonds are generally longer than the Na−O(carbonyl) bonds.[31] Here, one of the two Na−O(carbonyl) bonds is indeed shorter than the Na−O(ether) bonds (2.2116(18) Å), while the other is of comparable length with the shorter Na−O(ether) (2.4015(19) Å). The relative elongation of the latter Na−O(carbonyl) bond can be brought into connection with its surroundings in the crystal: it acts as an acceptor of a hydrogen bond with a water molecule (−H···O hydrogen bond of 2.92 Å). This water molecule also forms an O−H···N hydrogen bond (2.91 Å) with a nitrogen atom of a phenanthridine substituent of the same molecule (Figure 8b). Along with the water molecule, the structure also contains two symmetrically independent molecules of acetonitrile. Of these, one is included inside the calixarene *cone* similarly as in the structure of **L1**·2MeCN·0.5H_2O (Figures 8b, S5, and S6b, Supporting Information). The other acetonitrile molecule, as well as the perchlorate anion, is positioned in the spaces between the complex cations and binds solely through weak C−H···O and C−H···N hydrogen bonding contacts.

Molecular Dynamics Simulations of L1 and L2 Complexes. The calixarene complexes whose formation in different solvents was experimentally observed were also investigated by molecular dynamics simulations.

In the case of the Li**L1**$^+$ complex, the inclusion of an acetonitrile molecule was observed even during the preproduction phase of computation. During the production phase, the hydrophobic cavity was constantly occupied with acetonitrile molecules and the exchange dynamics was slow on MD time scale (Figure S71, Table S6, Supporting Information). During 94% of the simulation time, the bound solvent molecules were oriented with the methyl group pointing toward the cation forming a Li**L1**MeCN$^+$ complex (Figure 9a), while in the remaining period the nitrile group coordinated the lithium cation through the calixarene *cone* (the corresponding complex is denoted as Li**L1**MeCN′$^+$, Figure 9b). Similar binding mode was already observed.[33,35] Cation coordination by the MeCN nitrile group was reflected in the increase of the cation-$MeCN_{included}$ interaction energy by 45 kJ mol^{-1} (Table S6, Supporting Information). However, such a binding mode decreased the **L1**-cation interaction by the same amount and the **L1**-$MeCN_{included}$ interaction by about 32 kJ mol^{-1}. That explains the prevalence of the Li**L1**MeCN$^+$ form during the simulation. For all other cations, only the adducts in which the nitrile group was oriented toward the bulk were observed (Figure 9c−f, Table S6, Supporting Information). All complexes had a regular *cone*-shaped *basket* (Table S6, Supporting Information) as a result of both the cation complexation and the inclusion of solvent molecules.

In the complexes of **L1** the metal ions were found to be bound by all ether oxygen atoms and various numbers of the other cation coordinating groups (Table S6, Supporting Information). A significant decrease in coordination by C═O groups with the increase in cation size was observed (Table S6, Supporting Information), ranging from Na^+ (1.99) and to Cs^+ (0.52), whereas it was opposite with the number of coordinating phenanthridine N atoms (from 0.36 for Na^+ to 1.84 to Cs^+). Such a trend is in line with that observed in the case of phenanthridine diaza-crown ether derivatives.[50] Interestingly, this is clearly reflected in the characteristic spectra of the **L1** complexes, as shown in Figure 10.

https://doi.org/10.1021/acsomega.3c06509
ACS Omega 2023, 8, 43074−43087

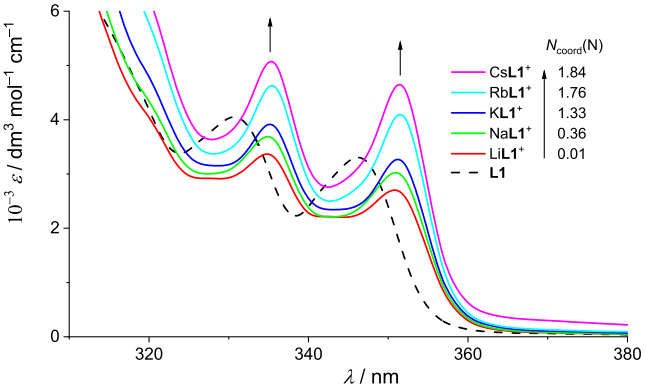

Figure 10. Dependence of characteristic absorption spectra of **L1** complexes in MeCN on the average number of phenanthridine N atoms coordinating the cation (MD results).

In all simulations of M**L2**$^+$ complexes in acetonitrile, the inclusion of solvent molecules was highly pronounced (Figures S72 and S73, Table S7, Supporting Information). In the adducts, the shape of the calixarene *basket* resembled the regular *cone*. The consequence of the difference in the cation binding sites of **L1** and **L2** (presence of amide or ester groups, respectively) is larger overall interaction energy of **L1** with cations which is about 60−120 kJ mol^{-1} more favorable than that of **L2** (Tables S6 and S7, Supporting Information), leading to up to 5 orders of magnitude larger stability constants of the complexes of former ligand (Tables 1 and 2). Regarding the dependence of the number of **L2** coordinating carbonyl groups and phenanthridine nitrogen atoms on the cation size, a trend similar to that described above for **L1** was observed (Table S7, Supporting Information).

Methanol adducts were observed for all investigated M−**L1**$^+$ complexes in over 90% of the simulation time (Figure S74, Tables S8 and S9, Supporting Information). Only in the case of Li$^+$ were two forms observed: the one in which MeOH hydroxyl group was pointed toward the bulk (84%) and the less favorable one with the opposite orientation (10%). For all other cations only the former adduct was observed (Figure S75, Supporting Information). Solvent exchange was fast, with 13 (Rb$^+$) to 28 (Li$^+$) solvent molecules being exchanged inside the hydrophobic cavity during the simulation time (Figure S74, Tables S8 and S9, Supporting Information). The coordination of alkali metal cations by **L1** in MeOH was similar as in MeCN: the number of coordinating C═O groups decreased from 1.9 (Na$^+$) to 1.5 (Rb$^+$), and the coordination through phenanthridine N atoms increased significantly, from 0.33 (Na$^+$) to 1.92 (Rb$^+$).

According to the MD simulations, the sodium complex of **L2** has a high affinity for methanol molecules (Figure S76, Table S10, Supporting Information). Only the formation of the Na**L2**MeOH$^+$ adduct was observed in which the methanol oxygen atom was oriented toward the bulk (Figure S77a, Supporting Information). Cation was coordinated by 1.9 carbonyl groups on average, and by 0.5 phenanthridine nitrogen atoms. The sodium cation-ligand interaction energy in the Na**L2**MeOH$^+$ complex was lower by 60 kJ mol^{-1} than in Na**L1**MeOH$^+$, a similar difference as in the binding energies of the corresponding MeCN adducts.

Although no inclusion of the solvent molecule was observed in free **L1**, EtOH adducts were formed with all studied M**L1**$^+$ complexes, and the dominant form was found to be in all cases the one in which the alkyl chain pointed toward the cation (Figure S78a,c,d, Supporting Information). The exchange of the ethanol molecules in hydrophobic cavities of **L1** complexes was fast on the MD time scale (Figure S79, Tables S11 and S12, Supporting Information). Unlike in the case of MeOH, a significant decrease in the adduct formation favorability with cation size was observed, as the % of free complex increased from 6 (Li$^+$) to 27 (K$^+$). This is supposedly due to the lower symmetry of the K$^+$ complex, which tends to disfavor adduct formation with bulkier EtOH (relative to MeOH). In the case of Na**L2**$^+$ complex, solvent adduct was observed 91% of the time with fast exchange (Table S13, Figures S80 and S81, Supporting Information).

Besides ether oxygen atoms, the coordination of cations in M**L1**EtOH$^+$ complexes was achieved primarily by the carbonyl groups where the lithium cation was bound by 1.3, the sodium cation by 1.9, and the potassium cation by 1.78 of these groups on average (Tables S11 and S12, Supporting Information). No phenanthridine nitrogen atom coordinated lithium cation in any of the complexes in ethanol, while in the sodium and potassium complexes, 0.4 and 1.4 nitrogen atoms of **L1** were on average attached to the cation, respectively. In Na**L2**EtOH$^+$ species, the sodium cation was coordinated by both carbonyl groups for almost all of the simulation time and, on average, by 0.25 nitrogen atom of phenanthridine substituents (Table S13, Supporting Information). The energy of the cation-ligand interaction was again weaker in Na**L2**EtOH$^+$ than in Na**L1**EtOH$^+$ by about 65 kJ mol^{-1}, which followed the difference in the experimentally determined stabilities of these complexes (Tables 1 and 2).

During most of the simulations of the **L1** complexes in DMF the solvent adducts were observed with slow exchange of the DMF molecules inside the calixarene cavity (Figure S82, Tables S14 and S15, Supporting Information). The ligand interaction of the included DMF molecule was more favorable than with acetonitrile, methanol, or ethanol, by 10−15 kJ mol^{-1}. As in the case of free **L1**, two M**L1**DMF$^+$ adducts (*cis* and *trans*) were present with all investigated cations (Figures S83a−c and S84, Supporting Information), where the *trans* adduct was in all cases the more stable one. Only in the case of Li$^+$ an additional adduct geometry was found (denoted as Li**L1**DMF"$^+$, Figure S83d, Supporting Information), in which the cation was directly coordinated by included solvent's C = O group. During the MD simulations, an additional type of lithium complexes were observed, in which the cation was only partially desolvated (Li**L1**DMF$^+$−DMF and Li**L1**DMF'$^+$−DMF, Figure S83e,f, Supporting Information). In these adducts, Li$^+$ was coordinated by the oxygen atom of DMF and by almost no C═O groups of **L1**.

The cations in M**L1**DMF$^+$ complexes were coordinated by all ether oxygen atoms, various number of carbonyl oxygen atoms, and, in the case of sodium and potassium complexes, by phenanthridine nitrogen atoms (Tables S14 and S15, Supporting Information). The number of coordinated carbonyl groups again increased with the cation size, while the number of bound nitrogen atoms was similar for sodium and potassium complexes (≈1).

Contrary to free **L1**, inclusion of DMSO molecules in the calixarene *basket* of the Na**L1**$^+$ complex was observed during 93% of the simulation time (Figure S85, Table S16, Supporting Information), whereby the exchange process was relatively fast. The interaction of the DMSO molecule with **L1** was as favorable as the interaction found in the DMF inclusion complexes.

https://doi.org/10.1021/acsomega.3c06509
ACS Omega 2023, 8, 43074−43087

The average coordination of Na^+ was accomplished through ether oxygens, nearly all C═O groups, and 0.24 phenanthridine nitrogen atoms. The inclusion of the DMSO molecule had almost no effect on the cation coordination (Table S16, Supporting Information).

Quantum-Chemical Computations. The initial set of geometries for the conformational analysis of Na**L1**$^+$ and Na**L2**$^+$ *in vacuo* and in discrete solvent was obtained by the statistical analysis of ab initio molecular dynamics trajectories. The corresponding structures were optimized at the B3LYP-D3/6-31G(d) level of theory. For these conformers, harmonic frequency calculations were carried out, and standard Gibbs energies were calculated. Conformational space of the complexes calculated in vacuo consists of many conformers. Four conformers of minimal energy, dependent on the sodium cation coordination number and binding atom types, were investigated in detail and can be distinguished using the assigned *binding mode vector*:

$$\{N_{O,ether}, N_{O,carbonyl}, N_N\}$$

where $N_{O,ether}$ and $N_{O,carbonyl}$ stand for the total number of coordinated ether and carbonyl oxygen atoms, and N_N is the total number of coordinated phenanthridine nitrogen atoms. Relative standard Gibbs energies of formation, $\Delta_f G^\circ_{rel}$, are given in Tables 3 and S17, Supporting Information, whereas the corresponding structures are presented in Figures 11 and S87, Supporting Information. For each of these conformers, several additional conformers that differ in orientation of two side chains exist.

Table 3. Relative Standard Gibbs Energies of Formation for Na$L1^+$ Complexes Calculated by Using B3LYP-D3/6-31G(d) Method (T = 298.15 K and p = 101,325 Pa)

conformer	$\Delta_f G^\circ_{rel}$/kJ mol^{-1}	coordination number for Na^+	binding mode vector
(a)	0.000	7	{4,1,2}
(b)	6.86	8	{4,2,2}
(c)	17.93	7	{4,2,1}
(d)	29.19	6	{4,0,2}

To investigate the solvent influence on conformational space of complexes, ab initio molecular dynamics with discrete solvent were performed. In each simulation, one solvent molecule was placed in the calixarene *cone*. This acetonitrile molecule symmetrizes the chemical environment for sodium cation ensuring the proper positioning and most commonly coordination number of 8. Two structures of the lowest electronic energy (harmonic frequency analysis would provide incorrect results because of the harmonic approximation breakdown) are presented in Figures S88 and S89, Supporting Information. Other conformers for both complexes are so much higher in energy that their presence in solvent is negligible.

CONCLUSIONS

The main aims and achievements of this work were:

1. To design and prepare highly sensitive fluorescent calixarene-based cation receptors. This task was accomplished by combining the features of the previously described ligands, namely the one functionalized with four phenanthridine subunits[41] and the other comprising four tertiary amide or ester moieties.[24,28,36] In addition, our objective was to enhance the solubility of receptors in polar organic solvents. Thus, we synthesized compounds **L1** and **L2** and obtained receptors whose fluorescence is significantly altered by the cation binding, and in the case of **L1** its affinity for alkali metal ions is much higher (in the case of sodium in acetonitrile about 2.5 orders of magnitude in terms of stability constants) than that of tetra-phenanthridine derivative. As was our intention, the Na**L1**$^+$ complex stability constant is in fact between those corresponding to tetra-phenanthridine[41] and tetra-tertiary-amide derivatives,[28] as can be clearly seen in Figure 12a.
2. To characterize in detail the ligands **L1** and **L2** and their cation binding processes from the structural and thermodynamic points of view. Therefore, crystal structures of **L1** and its complex with Na^+ were determined. Possible structures of the ligands and complex species in solution were proposed based on the results of molecular dynamics simulations and DFT computations. Thermodynamic parameters (equilibrium constants and the derived standard reaction Gibbs energies, as well as standard reaction enthalpies and entropies) of all studied binding processes were determined and thoroughly discussed.
3. To explore the solvent effect on the thermodynamics of studied reactions. For that reason, five solvents of different solvation properties and hydrogen-bonding abilities were examined. As illustrated in Figure 12b, the complex stabilities were found to be significantly (in some cases even hugely) solvent dependent as a consequence of differences in the solvation of the ligands, cations, and their complexes. In this respect, by carrying out the molecular dynamics simulations, it was shown that the inclusion of solvent molecule in the hydrophobic cavity of

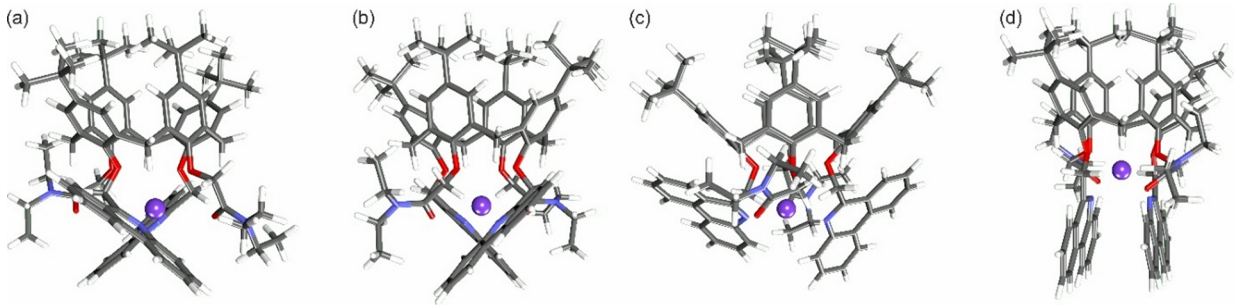

Figure 11. Conformers of **L1** in complex with Na^+ in dependence on sodium cation coordination number and binding atom types calculated by using B3LYP-D3/6-31G(d) method. (T = 298.15 K and p = 101,325 Pa) (a) {4,1,2}, (b) {4,2,2}, (c) {4,2,1}, and (d) {4,0,2}.

https://doi.org/10.1021/acsomega.3c06509
ACS Omega 2023, 8, 43074−43087

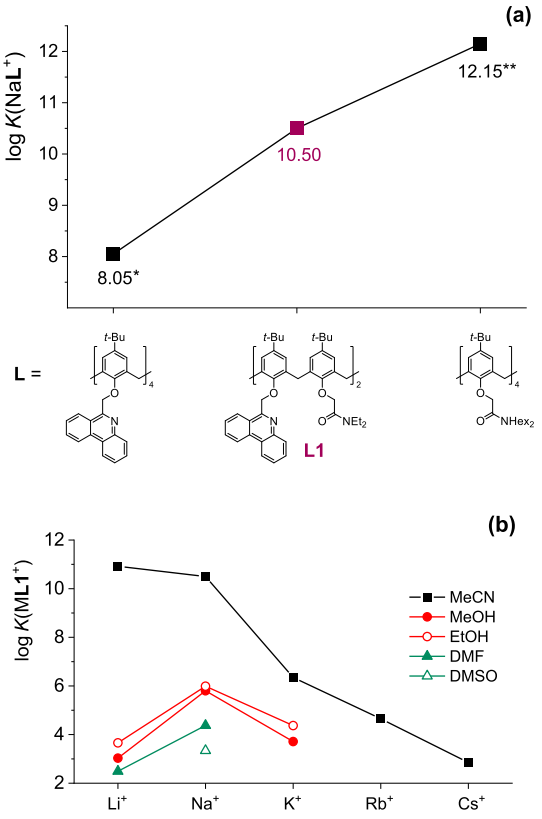

Figure 12. (a) Dependence of Na**L**$^+$ complex stability constants on calix[4]arene lower-rim substituents in MeCN, * from ref 41, ** from ref 28. (b) M**L1**$^+$ (M = Li, Na, K, Rb, Cs) complex stability constants as a function of the solvent used.

the free and complexed ligands plays an important role in determining the complexation equilibrium.

■ ASSOCIATED CONTENT

Supporting Information

The Supporting Information is available free of charge at https://pubs.acs.org/doi/10.1021/acsomega.3c06509.

Experimental and computational procedures: synthesis of compound **1**; ^{1}H, ^{13}C NMR and IR spectra of compounds **L1** and **L2**; additional spectrophotometric, fluorimetric, and calorimetric titrations; molecular dynamics simulations and DFT calculations; additional details regarding crystal structures; crystallographic data in CIF format (PDF)

■ AUTHOR INFORMATION

Corresponding Author

Vladislav Tomišić − *Department of Chemistry, Faculty of Science, University of Zagreb, 10 000 Zagreb, Croatia;* orcid.org/0000-0002-1191-2123; Email: vtomisic@chem.pmf.hr

Authors

Katarina Leko − *Department of Chemistry, Faculty of Science, University of Zagreb, 10 000 Zagreb, Croatia*

Andrea Usenik − *Department of Chemistry, Faculty of Science, University of Zagreb, 10 000 Zagreb, Croatia;* orcid.org/0000-0003-1995-8705

Nikola Cindro − *Department of Chemistry, Faculty of Science, University of Zagreb, 10 000 Zagreb, Croatia*

Matija Modrušan − *Department of Chemistry, Faculty of Science, University of Zagreb, 10 000 Zagreb, Croatia*

Josip Požar − *Department of Chemistry, Faculty of Science, University of Zagreb, 10 000 Zagreb, Croatia;* orcid.org/0000-0002-2521-9311

Gordan Horvat − *Department of Chemistry, Faculty of Science, University of Zagreb, 10 000 Zagreb, Croatia*

Vladimir Stilinović − *Department of Chemistry, Faculty of Science, University of Zagreb, 10 000 Zagreb, Croatia;* orcid.org/0000-0002-4383-5898

Tomica Hrenar − *Department of Chemistry, Faculty of Science, University of Zagreb, 10 000 Zagreb, Croatia;* orcid.org/0000-0002-4570-0524

Complete contact information is available at: https://pubs.acs.org/10.1021/acsomega.3c06509

Author Contributions

†K.L. and A.U. contributed equally.

Notes

The authors declare no competing financial interest.

■ ACKNOWLEDGMENTS

This research was funded by Croatian Science Foundation (project MacroSol, grant number IP-2019-04-9560) and European Regional Development Fund (infrastructural project CIuK, grant number KK.01.1.1.02.0016)

■ REFERENCES

(1) *Calixarenes and Beyond*, Neri, P., Sessler, J. L., Wang, M.-X., Eds.; Springer International Publishing: Cham, Switzerland, 2016.

(2) Gutsche, C. D. *Calixarenes: An Introduction*, 2nd ed.; The Royal Society of Chemistry: Cambridge, U.K. 2008.

(3) Baldini, L., Sansone, F., Casnati, A., Ungaro, R. In *Supramolecular Chemistry: from Molecules to Nanomaterials*; Steed, J. W., Gale, P. A., Eds.; John Wiley & Sons: Chichester, 2012; 863−894.

(4) *Calixarenes 2001*; Asfari, Z., Böhmer, V., Harrowfield, J., Vicens, J., Eds.; Kluwer Academic Publishers: Dordrecht, Netherlands, 2001.

(5) Homden, D. M.; Redshaw, C. The Use of Calixarenes in Metal-Based Catalysis. *Chem. Rev.* **2008**, *108* (12), 5086−5130.

(6) Sviben, I.; Galić, N.; Tomišić, V.; Frkanec, L. Extraction and Complexation of Alkali and Alkaline Earth Metal Cations by Lower-Rim Calix[4]arene Diethylene Glycol Amide Derivatives. *New J. Chem.* **2015**, *39* (8), 6099−6107.

(7) Arnaud-Neu, F.; Barrett, G.; Fanni, S.; Marrs, D.; McGregor, W.; McKervey, M. A.; Schwing-Weill, M.-J.; Vetrogon, V.; Wechsler, S. Extraction and Solution Thermodynamics of Complexation of Alkali and Alkaline-Earth Cations by Calix[4]arene Amides. *J. Chem. Soc., Perkin Trans.* **1995**, *2*, 453−461.

(8) Evtugyn, G. A.; Stoikova, E. E.; Shamagsumova, R. V. Molecular Receptors and Electrochemical Sensors Based on Functionalized Calixarenes. *Russ. Chem. Rev.* **2011**, *79* (12), 1071−1097.

(9) O'Connor, K. M.; Arrigan, D. W. M.; Svehla, G. Calixarenes in Electroanalysis. *Electroanalysis* **1995**, *7* (3), 205−215.

(10) Forster, R. J., Keyes, T. E. *Ion-Selective Electrodes in Environmental Analysis in Encyclopedia of Analytical Chemistry*; John Wiley & Sons: New York, 2006.

(11) Kim, J. S.; Quang, D. T. Calixarene-Derived Fluorescent Probes. *Chem. Rev.* **2007**, *107* (9), 3780−3799.

(12) Kumar, R.; Sharma, A.; Singh, H.; Suating, P.; Kim, H. S.; Sunwoo, K.; Shim, I.; Gibb, B. C.; Kim, J. S. Revisiting Fluorescent Calixarenes: From Molecular Sensors to Smart Materials. *Chem. Rev.* **2019**, *119* (16), 9657−9721.

(13) Mako, T. L.; Racicot, J. M.; Levine, M. Supramolecular Luminescent Sensors. *Chem. Rev.* **2019**, *119* (1), 322−477.
(14) Kumar, R., Jung, Y., Kim, J. S. in *Calixarenes and Beyond*; Neri, P., Sessler, J. L., Wang, M.-X., Eds.; Springer International Publishing: Cham, Switzerland, 2016; 743−760.
(15) Massi, M.; Ogden, M. I. Luminescent Lanthanoid Calixarene Complexes and Materials. *Materials* **2017**, *10* (12), 1369.
(16) Rebilly, J.-N.; Colasson, B.; Bistri, O.; Over, D.; Reinaud, O. Biomimetic cavity-based metal complexes. *Chem. Soc. Rev.* **2015**, *44* (2), 467−489.
(17) Schühle, D. T.; Peters, J. A.; Schatz, J. Metal Binding Calixarenes with Potential Biomimetic and Biomedical Applications. *Coord. Chem. Rev.* **2011**, *255* (23−24), 2727−2745.
(18) Pan, Y.; Hu, X.; Guo, D. Biomedical Applications of Calixarenes: State of the Art and Perspectives. *Angew. Chem., Int. Ed.* **2021**, *60* (6), 2768−2794.
(19) Nimse, S. B.; Kim, T. Biological Applications of Functionalized Calixarenes. *Chem. Soc. Rev.* **2013**, *42* (1), 366−386.
(20) Matthews, S. E., Beer, P. D. in *Calixarenes in the Nanoworld*; Vicens, J., Harrowfield, J., Eds.; Springer: Dordrecht, Netherlands, 2001; 109−133.
(21) Kongor, A. R.; Mehta, V. A.; Modi, K. M.; Panchal, M. K.; Dey, S. A.; Panchal, U. S.; Jain, V. K. Calix-Based Nanoparticles: A Review. *Top. Curr. Chem.* **2016**, *374* (3), 28.
(22) Rudkevich, D. M. In *Calixarenes in the Nanoworld*; Vicens, J., Harrowfield, J., Eds.; Springer: Dordrecht, Netherlands, 2001; 151−172.
(23) Baldini, L.; Casnati, A.; Sansone, F. Multivalent and Multifunctional Calixarenes in Bionanotechnology. *Eur. J. Org. Chem.* **2020**, *2020* (32), 5056−5069.
(24) Arnaud-Neu, F.; Collins, E. M.; Deasy, M.; Ferguson, G.; Harris, S. J.; Kaitner, B.; Lough, A. J.; McKervey, M. A.; Marques, E. Synthesis, X-ray Crystal Structures, and Cation-Binding Properties of Alkyl Calixaryl Esters and Ketones, a New Family of Macrocyclic Molecular Receptors. *J. Am. Chem. Soc.* **1989**, *111* (23), 8681−8691.
(25) Śliwa, W.; Girek, T. Calixarene complexes with metal ions. *J. Incl. Phenom. Macrocycl. Chem.* **2010**, *66* (1−2), 15−41.
(26) Danil de Namor, A. F.; Cleverley, R. M.; Zapata-Ormachea, M. L. Thermodynamics of Calixarene Chemistry. *Chem. Rev.* **1998**, *98* (7), 2495−2526.
(27) Danil de Namor, A. F. In *Calixarenes 2001*; Asfari, Z., Böhmer, V., Harrowfield, J., Vicens, J., Eds.; Kluwer Academic Publishers: Dordrecht, Netherlands, 2001; 346−364.
(28) Horvat, G.; Frkanec, L.; Cindro, N.; Tomišić, V. A comprehensive study of the complexation of alkali metal cations by lower rim, calix[4]arene amide derivatives. *Phys. Chem. Chem. Phys.* **2017**, *19* (35), 24316−24329.
(29) Požar, J.; Cvetnić, M.; Usenik, A.; Cindro, N.; Horvat, G.; Leko, K.; Modrušan, M.; Tomišić, V. The Role of Triazole and Glucose Moieties in Alkali Metal Cation Complexation by Lower-Rim Tertiary-Amide Calix[4]arene Derivatives. *Molecules* **2022**, *27* (2), 470.
(30) Požar, J.; Nikšić-Franjić, I.; Cvetnić, M.; Leko, K.; Cindro, N.; Pičuljan, K.; Borilović, I.; Frkanec, L.; Tomišić, V. Solvation effect on complexation of alkali metal cations by a calix[4]arene ketone derivative. *J. Phys. Chem. B* **2017**, *121* (36), 8539−8550.
(31) Horvat, G.; Stilinović, V.; Hrenar, T.; Kaitner, B.; Frkanec, L.; Tomišić, V. An Integrated Approach (Thermodynamic, Structural and Computational) to the Study of Complexation of Alkali-Metal Cations by a Lower-Rim Calix[4]arene Amide Derivative in Acetonitrile. *Inorg. Chem.* **2012**, *51* (11), 6264−6278.
(32) Arduini, A.; Ghidini, E.; Pochini, A.; Ungaro, R.; Andreetti, G. D.; Calestani, G.; Ugozzoli, F. *p-t*-Butylcalix[4]arene tetra-acetamide: a new strong receptor for alkali cations [1]. *J. Incl. Phenomen.* **1988**, *6* (2), 119−134.
(33) Danil de Namor, A. F.; Chahine, S.; Kowalska, D.; Castellano, E. E.; Piro, O. E. Selective Interaction of Lower Rim Calix[4]arene Derivatives and Bivalent Cations in Solution. Crystallographic Evidence of the Versatile Behavior of Acetonitrile in Lead(II) and Cadmium(II) Complexes. *J. Am. Chem. Soc.* **2002**, *124* (43), 12824−12836.
(34) Požar, J.; Preočanin, T.; Frkanec, L.; Tomišić, V. Thermodynamics of Complexation of Alkali Metal Cations by a Lower-Rim Calix[4]arene Amino Acid Derivative. *J. Solution Chem.* **2010**, *39* (6), 835−848.
(35) Horvat, G.; Stilinović, V.; Kaitner, B.; Frkanec, L.; Tomišić, V. The Effect of Specific Solvent−Solute Interactions on Complexation of Alkali-Metal Cations by a Lower-Rim Calix[4]arene Amide Derivative. *Inorg. Chem.* **2013**, *52* (21), 12702−12712.
(36) Danil de Namor, A. F.; Matsufuji-Yasuda, T. T.; Zegarra-Fernandez, K.; Webb, O. A.; El Gamouz, A. An Enchiridion of Supramolecular Thermodynamics: Calix[*N*]arene (*N* = 4,5,6) Tertiary Amide Derivatives and Their Ionic Recognition. *Croat. Chem. Acta* **2013**, *86* (1), 1−19.
(37) Leko, K.; Bregović, N.; Cvetnić, M.; Cindro, N.; Tranfić Bakić, M.; Požar, J.; Tomišić, V. Complexation of Alkali Metal Cations by a Tertiary Amide Calix[4]Arene Derivative in Strongly Cation Solvating Solvents. *Croat. Chem. Acta* **2017**, *90* (2), 307−314.
(38) Danil de Namor, A. F.; Chahine, S.; Castellano, E. E.; Piro, O. E. Solvent Control on the Selective, Nonselective, and Absent Response of a Partially Substituted Lower Rim Calix(4)arene Derivative for Soft Metal Cations (Mercury(II) and Silver(I)). Structural and Thermodynamic Studies. *J. Phys. Chem. A* **2005**, *109* (30), 6743−6751.
(39) de Araujo, A. S.; Piro, O. E.; Castellano, E. E.; Danil de Namor, A. F. Combined Crystallographic and Solution Molecular Dynamics Study of Allosteric Effects in Ester and Ketone *p-tert*-Butylcalix[4]arene Derivatives and Their Complexes with Acetonitrile, Cd(II), and Pb(II). *J. Phys. Chem. A* **2008**, *112* (46), 11885−11894.
(40) Danil de Namor, A. F.; de Sueros, N. A.; McKervey, M. A.; Barrett, G.; Neu, F. A.; Schwing-Weill, M. J. The solution thermodynamics of ethyl *p-tert*-butylcalix[4]arene tetraacetate and its alkali metal complexes in acetonitrile and methanol. *J. Chem. Soc., Chem. Commun.* **1991**, 1546−1548.
(41) Tranfić Bakić, M.; Jadreško, D.; Hrenar, T.; Horvat, G.; Požar, J.; Galić, N.; Sokol, V.; Tomaš, R.; Alihodžić, S.; Žinić, M.; Frkanec, L.; Tomišić, V. Fluorescent phenanthridine-based calix[4]arene derivatives: synthesis and thermodynamic and computational studies of their complexation with alkali-metal cations. *RSC Adv.* **2015**, *5* (30), 23900−23914.
(42) Bregović, N.; Cindro, N.; Frkanec, L.; Tomišić, V. Complexation of fluoride anion and its ion pairs with alkali metal cations by tetra-substituted lower rim calix[4]arene tryptophan derivative. *Supramol. Chem.* **2016**, *28* (5−6), 608−615.
(43) Tranfić Bakić, M.; Leko, K.; Cindro, N.; Portada, T.; Hrenar, T.; Frkanec, L.; Horvat, G.; Požar, J.; Tomišić, V. Synthesis of Fluorescent Diphenylantracene-Based Calix[4]Arene Derivatives and Their Complexation with Alkali Metal Cations. *Croat. Chem. Acta* **2017**, *90* (4), 711−725.
(44) Raszeja, L.; Maghnouj, A.; Hahn, S.; Metzler-Nolte, N. A Novel Organometallic Re^{I} Complex with Favourable Properties for Bioimaging and Applicability in Solid-Phase Peptide Synthesis. *ChemBioChem* **2011**, *12* (3), 371−376.
(45) Gans, P.; Sabatini, A.; Vacca, A. Investigation of equilibria in solution. Determination of equilibrium constants with the HYPERQUAD suite of programs. *Talanta* **1996**, *43* (10), 1739−1753.
(46) Gans, P.; Sabatini, A.; Vacca, A. Simultaneous Calculation of Equilibrium Constants and Standard Formation Enthalpies from Calorimetric Data for Systems with Multiple Equilibria in Solution. *J. Solution Chem.* **2008**, *37* (4), 467−476.
(47) Briggner, L.-E.; Wadsö, I. Test and calibration processes for microcalorimeters, with special reference to heat conduction instruments used with aqueous systems. *J. Biochem. Biophys. Meth.* **1991**, *22* (2), 101−118.
(48) *CrysAlisPro 1.171.41.92a*; Rigaku Oxford Diffraction: Oxford, UK, 2020.
(49) Marcus, Y. *Ion Properties*; M. Dekker: New York, 1997.

https://doi.org/10.1021/acsomega.3c06509
ACS Omega 2023, 8, 43074−43087

(50) Alihodžić, S.; Žinić, M.; Klaić, B.; Kiralj, R.; Kojić-Prodić, B.; Herceg, M.; Cimerman, Z. Fluoroionophores with Phenanthridinyl Units. *Tetrahedron Lett.* **1993**, *34* (51), 8345−8348.

https://doi.org/10.1021/acsomega.3c06509
ACS Omega 2023, 8, 43074−43087